Plasma Chemistry and Plasma Processing (2023) 43:1907–1919
https://doi.org/10.1007/s11090-023-10345-8

ORIGINAL PAPER

Plasma Nitrogen Fixation: NO_x Synthesis in MnO_x/Al_2O_3 Packed-Bed Dielectric Barrier Discharge

Tian-Qi Zhang[1,2] · Xiao-Song Li[1,2] · Jing-Lin Liu[2] · Xiao-Qiong Wen[1] · Ai-Min Zhu[1,2]

Received: 5 May 2023 / Accepted: 8 June 2023 / Published online: 26 June 2023

Abstract
The plasma nitrogen fixation for NO_x synthesis from N_2 and O_2 in MnO_x/Al_2O_3 packed-bed dielectric barrier discharge (DBD) and an enhanced effect of MnO_x/Al_2O_3 catalyst are reported. At N_2 content of 50% and *SEI* of ~ 16 kJ/mol (flow rate of 800 SCCM and discharge power of ~ 9.5 W), NO_x production rates are 0.28 SCCM for Al_2O_3 and 0.42 SCCM for MnO_x/Al_2O_3, and improved by ~ 60% due to the enhanced effect of MnO_x/Al_2O_3. The enhanced effect becomes more significant at lower specific energy input (SEI) or higher N_2 content (lower O_2 content). The MnO_x/Al_2O_3-packed DBD features much more and lower-intensity micro-discharges, larger total capacitance, greater peak-to-peak charge, and higher vibrational temperature of N_2 than the Al_2O_3-packed DBD. The surface role of MnO_x/Al_2O_3 catalyst in the enhanced effect was disclosed by two-step surface reaction processes and in-situ temperature programed desorption for the adsorbed species of the first step.

Keywords Dielectric barrier discharge · Plasma catalysis · Nitrogen fixation · NO_x synthesis

Introduction

The use of plasma for nitrogen fixation has attracted great attention in reduction of N_2 to ammonia with hydrogen or oxidation of N_2 to nitrogen oxides (NO_x, $NO + NO_2$) with oxygen [1–10]. The oxidative nitrogen fixation is superior to reductive nitrogen fixation in the cost of feed gas, because air can be directly used for NO_x synthesis. The NO_x production rate is limited by N_2 and O_2 dissociation due to high bond energy of N_2 (9.8 eV) and O_2 (5.2 eV). Due to the relatively low electron energy in atmospheric-pressure plasma [11], most of the molecules are in electronically and vibrationally excited states (O_2^*, N_2^*),

✉ Xiao-Qiong Wen
wenxq@dlut.edu.cn

✉ Ai-Min Zhu
amzhu@dlut.edu.cn

[1] Key Laboratory of Materials Modification by Laser, Ion and Electron Beams, Dalian University of Technology, Ministry of Education, Dalian 116024, China

[2] Laboratory of Plasma Physical Chemistry, Dalian University of Technology, Dalian 116024, China

rather than dissociation to N and O atoms, despite they are considered as the important species from a plausible plasma radical-involving mechanism [12].

The early attempt to promote the reaction of excited molecules was made by the combination of plasma with catalysts using inductively coupled plasma (ICP) at low pressure. For example, Rapakoulias et al. [13] found the enhanced effect of WO_3 and MoO_3 catalysts on NO synthesis and suggested that vibrationally excited nitrogen molecule underwent dissociative adsorption on the catalyst surface and then reacted with oxygen. Gicquel et al. [14] proposed that N atoms or excited N_2 molecules reacted with WO_3 and MoO_3 catalysts to form MoO_3–N (adsorbed) or MoO_3–N_2^*(adsorbed) and then NO was released. However, the excited N_2 molecules collided with the oxide surface would prefer energy relaxation instead of dissociation due to the very low sticking probability on oxides.

Recently, dielectric barrier discharge (DBD) plasma has been used to study the plasma catalytic synthesis of NO_x. Patil et al. [15] investigated the effect of various metal oxides (WO_3, PbO, CuO, Co_3O_4, NiO, MoO_3 and V_2O_5) supported on Al_2O_3 on NO_x synthesis in a DBD reactor. The WO_3/Al_2O_3 catalyst increased the NO_x concentration by about 10% compared to Al_2O_3 and the authors thought that the vibrationally excited nitrogen molecules have a reaction with the mobile oxygen species on the catalyst surface. Ma et al. [16] investigated the effect of Al_2O_3 and $BaTiO_3$ packing on NO_x synthesis in a DBD reactor. They proposed that the enhanced production of NO_x was attributed to the increased electron energy due to the presence of packing materials instead of surface-reaction contribution. In our previous work [17], it was found that higher temperatures (> 623 K) were beneficial for the formation of NO_x on Cu-ZSM-5 catalyst in a DBD reactor. The reaction of nitrogen species with the activated O_2 or adsorbed atomic oxygen on Cu active sites at higher temperatures may improve the NO formation. Taken together, the studies on plasma nitrogen fixation for NO_x synthesis have rather little reported, and the contribution of surface reaction is still hitherto unknown.

The aim of this work is to study, for the first time, NO_x synthesis from N_2 and O_2 in MnO_x/Al_2O_3-packed DBD plasma, because MnO_x with strong reducibility, multiple oxidation states and oxygen vacancies [18], has a potential to activate the oxygen species. In this work, based upon the comparison with the empty and Al_2O_3-packed DBD, an enhanced effect on NO_x production in MnO_x/Al_2O_3-packed DBD is found. The enhanced effect becomes more significant at lower specific energy input (*SEI*) or higher N_2 content (lower O_2 content). To gain an insight on the enhanced effect of MnO_x/Al_2O_3 catalyst, its electrical discharge characteristics, optical emission spectra and surface role of MnO_x/Al_2O_3 catalyst were further investigated.

Experimental Methods

Figure 1 is the schematic diagram of the experimental setup. The DBD reactor is coaxial and consists of a quartz tube (10 mm outer diameter and 8 mm inner diameter), a high voltage electrode (3-mm-diameter stainless steel rod) and a ground electrode (30 mm-height stainless steel mesh). The high voltage electrode was powered by an AC power supply with frequency of 13.3 kHz (CTP-2000 K, Nanjing Suman). The digital oscilloscope (Tektronix MDO3014) recorded signals from a high voltage probe (Tektronix P6015A) and a passive probe connected with a 51 Ω sampling resistor or a 0.22 μF sampling capacitor, then voltage-current waveforms or charge–voltage Lissajous figures were obtained. The input power (P_{in}) was directly measured by a wattmeter from the power supply, and the discharge

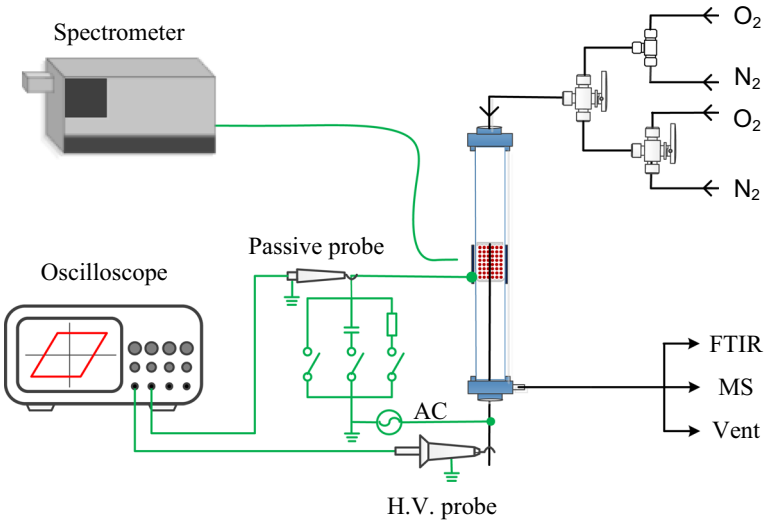

Fig. 1 Schematic diagram of the experimental setup. *AC* alternating current, *H.V.* high voltage, *FTIR* Fourier transform infrared spectroscopy, *MS* mass spectrometer

power was calculated from the Lissajous figure. One of three types of circuits, including a sampling resistor, sampling capacitor and short circuit, was chosen to connect the switch without stopping discharge. The specific energy input (*SEI*) is defined as,

$$SEI = \frac{P_{dis}}{F_{in}}$$

where P_{dis} and F_{in} are the discharge power and the gas inlet flow rate, respectively.

Optical emission spectroscopy (OES) was used for the plasma diagnostic. The fiber-optic probe is perpendicular to the DBD reactor, and the distance between the reactor wall and fiber is 45 mm. The light emitted from the DBD plasma was measured by a high-resolution spectrometer (Andor Shamrock SR-750, 1200 grooves/mm grating, 50 μm width slit) along with an intensified charge-coupled device (ICCD) detector (Andor iStar DH334). The spectrum was recorded with exposure time of 0.5 s and 20 accumulations. The second positive system of N_2 ($C^3\Pi_u \rightarrow B^3\Pi_g$) was used to evaluate the rotational (T_r) and vibrational (T_v) temperatures by the method reported previously [19]. Fig. S1 gives an example of experimental and fitted spectra for evaluating the rotational and vibrational temperatures.

N_2 and O_2 gases (purity 99.999%), whose flow rates were adjusted by mass flow controllers, were fed separately or mixed into the reactor. The outlet gas from the reactor flowed into the gas cell of the Fourier transform infrared (FT-IR) spectrometer (IGS gas analyzer, Thermo Fisher, USA). The concentrations of NO, NO_2, N_2O and O_3 were monitored online by the FT-IR spectrometer, equipped with an MCT detector, in a scanning range of 600–4000 cm^{-1} and at a resolution of 0.5 cm^{-1}. N_2 was used to purge the gas cell and gas pipelines for removing air and water before measurement. The time for data collection is more than 20 min, which is enough to reach a steady concentration of the products even under a minimal flow rate (400 SCCM).

It is needed to note, there exist N_2O and NO_2 impurities in NO standard gas due to NO decomposition at high pressures of gas cylinder. Hence, the calibration curve of NO was obtained by using N_2-balanced NO_2 standard gas, which went through a molybdenum converter to obtain accurate concentrations of NO for NO calibration. The concentrations of NO and N_2O were quantified in the range of 1880–1960 cm^{-1} and 2140–2280 cm^{-1}, respectively. To quantify NO_2, 1880–1960 cm^{-1} (below 1000 ppm) and 2820–2950 cm^{-1} (between 1000 and 10,000 ppm) were employed. The concentration calibration curves of NO and NO_2 are shown in Fig. S2. Figure 2 shows a typical FTIR spectra. Because NO is easily oxidized to NO_2 in O_2-containing gas, the concentration of NO_x is defined as the sum of NO and NO_2 and it was adopted to evaluate the reaction performance.

The MnO_x/Al_2O_3 catalysts were prepared by incipient wetness impregnation of γ-Al_2O_3 pellets (diameter ~ 1 mm) in manganese nitrate solution for 12 h at room temperature. The impregnated samples were dried at 120 °C for 4 h and then calcined at 450 °C in static air for 4 h. The nominal content in Mn of the MnO_x/Al_2O_3 catalyst is 9 wt%. The X-ray diffraction (XRD) patterns were obtained by using D8 Advance X-ray Diffractometer (Bruker, Germany, Cu *K*α, 0.154056 nm). The XRD profile of the as-prepared MnO_x/Al_2O_3 is shown in Fig. S3, showing that the MnO_x with weak crystallinity of β-MnO_2. The morphology of MnO_x/Al_2O_3 catalysts was observed by a field emission scanning electron microscopy (FE-SEM, JSM-7900F, JEOL LTD, Japan). The SEM images with energy dispersive spectroscopy (EDS) analysis of MnO_x/Al_2O_3, as shown in Fig. S4, indicate an even dispersion of MnO_x on the Al_2O_3 support. Before plasma reaction, the catalysts packed into the DBD reactor were in-situ purified with 100 SCCM N_2 at 400 °C for 0.5 h using a tubular furnace, then cooled down to room temperature for starting the plasma catalytic reaction.

To gain an insight into the MnO_x/Al_2O_3 catalyst enhanced NO_x synthesis, the plasma catalytic reaction was separated into two steps. At the first step, the catalyst was treated by one of N_2 and O_2 plasmas for 20 min with a flow rate of 100 SCCM at $P_{in} = 20$ W; at the second step, the catalyst was treated by the other one at the same flow rate and P_{in} as the

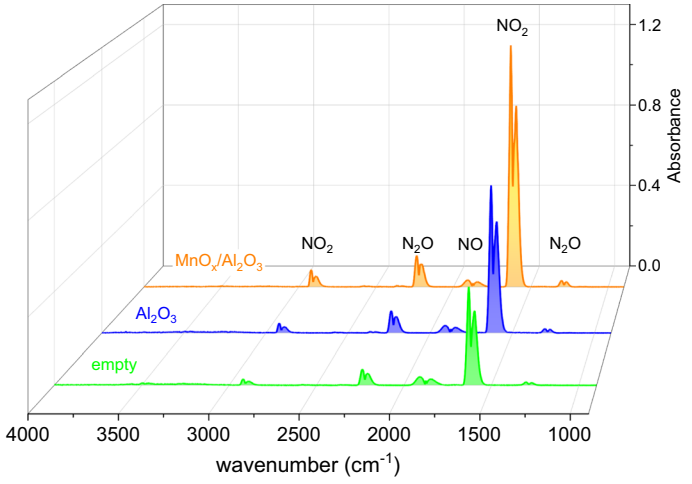

Fig. 2 The FTIR spectra of the products in the empty, Al_2O_3-packed and MnO_x/Al_2O_3-packed DBD reactor at discharge time of 20 min. Conditions: $F_{in} = 400$ SCCM, 50% N_2 + 50% O_2, $P_{in} = 20$ W (P_{dis} of empty, Al_2O_3-packed and MnO_x/Al_2O_3-packed DBD are 9.6, 9.4 and 9.9 W, respectively)

first step. For the MnO_x/Al_2O_3 catalyst, the gaseous and surface products of the second step (N_2 plasma) after O_2 adsorption or O_2 plasma for the first step were compared. Moreover, the adsorbed species of the first step were analyzed by in-situ temperature programed desorption (TPD). After the first step, the in-situ TPD was carried out from room temperature to 400 °C at a ramp rate of 10 °C/min, and kept at 400 °C for 30 min in Ar gas of 100 SCCM. A mass spectrometer (MS, Hiden HPR20, UK) with a heated (at 393 K) quartz inert capillary inlet was used to monitor online the products during the two-step surface reaction processes and the in-situ TPD.

Results and Discussion

Enhanced Effect of MnO_x/Al_2O_3 Catalyst on NO_x Synthesis

Figure 3 shows the NO_x concentrations produced in the empty, Al_2O_3-packed, or MnO_x/Al_2O_3-packed DBD reactor at flow rate of 600 SCCM and 50% nitrogen content. The NO_x concentrations of the empty and Al_2O_3-packed DBD are very close at discharge power of about 9.5 W (Case A in Fig. 3) being 506 and 513 ppm, respectively. Nonetheless, the NO_x concentration increases significantly to 755 ppm in MnO_x/Al_2O_3-packed DBD, which is much higher than those of the empty and Al_2O_3-packed DBD. Likewise, at discharge power of about 17 W (Case B in Fig. 3), NO_x concentration of the MnO_x/Al_2O_3-packed DBD is the highest, reaching 1300 ppm. This demonstrates that MnO_x/Al_2O_3 catalyst has an enhanced effect on NO_x production.

By varying discharge power or flow rate, the effect of *SEI* on NO_x concentration and production rate in the Al_2O_3-packed and MnO_x/Al_2O_3-packed DBD at 50% nitrogen content is presented in Fig. 4. At a fixed flow rate, the residence time is kept at constant and thus the effect of *SEI* by changing discharge power is a single-factor examination. The *SEI* means the average energy absorbed by each molecule for activation and reaction in plasma. The increase of *SEI* leads to a rise in electron density, so higher *SEI* is benefit to the formation of more active species of nitrogen and oxygen to promote the production of NO_x. As a result, NO_x concentration and production rate increase rapidly with *SEI* by changing discharge power (Fig. 4a), which accords with the literature reported in plasma catalytic ammonia synthesis [20]. The *SEI* can

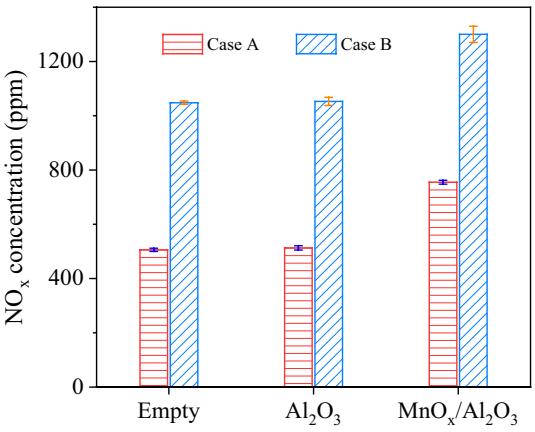

Fig. 3 The NO_x concentration produced in the DBD reactor. Conditions: $F_{in}=600$ SCCM, 50% $N_2+50\%$ O_2. Case A: P_{dis} of empty, Al_2O_3-packed and MnO_x/Al_2O_3-packed DBD at $P_{in}=20$ W are 9.6, 9.5 and 9.7 W, respectively; Case B: P_{dis} of empty, Al_2O_3-packed and MnO_x/Al_2O_3-packed DBD at $P_{in}=30$ W are 16.8, 16.9 and 17.3 W, respectively

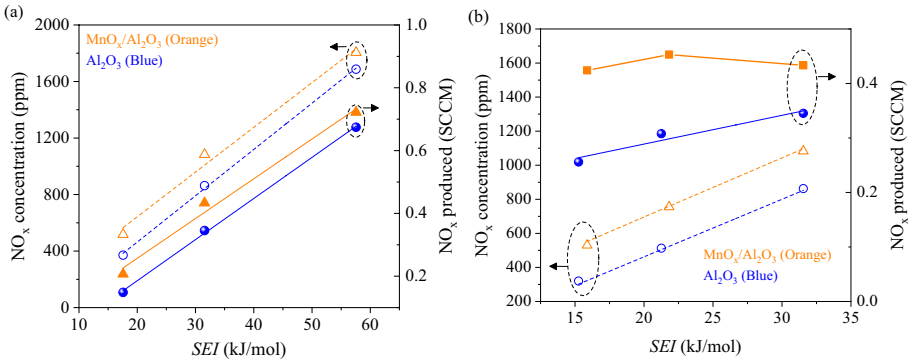

Fig. 4 NO_x concentration and production rate versus *SEI* by changing, **a** discharge power and **b** flow rate. Conditions: 50% N_2 + 50% O_2. **a** F_{in} = 400 SCCM, P_{dis} of MnO_x/Al_2O_3 (Al_2O_3) are 5.2 (5.2), 9.6 (9.4) and 17.3 (17.1) W at P_{in} of 15, 20 and 30 W, respectively; **b** P_{in} = 20 W, P_{dis} of MnO_x/Al_2O_3 (Al_2O_3) are 9.9 (9.4), 9.7 (9.5) and 9.5 (9.1) W for F_{in} of 400, 600 and 800 SCCM, respectively

also be varied by adjusting flow rate when the power is fixed, however, the residence time is changed accordingly. Interestingly, as shown in Fig. 4b (by changing flow rate), the NO_x production rate rises very slow with *SEI* for Al_2O_3-packed, and even turns to decrease slightly after a small increase for MnO_x/Al_2O_3-packed. Figure 4b is a result of combined effect of *SEI* and residence time. The long residence time brings about further oxidation of NO_x–N_2O_5 [21], or NO decomposition into N_2 and O_2 [22, 23], which weakens or overwhelms the positive effect of *SEI* on NO_x production.

Moreover, Fig. 4 shows that NO_x concentration and production rate of MnO_x/Al_2O_3 are higher than that of Al_2O_3 at the same *SEI*, supporting again the enhanced effect of MnO_x/Al_2O_3 catalyst. Especially at lower *SEI*, MnO_x/Al_2O_3 catalyst provides greater enhanced effect on NO_x production rate. For example, at *SEI* of ~ 16 kJ/mol (Fig. 4b), NO_x production rates are 0.26 SCCM for Al_2O_3 and 0.42 SCCM for MnO_x/Al_2O_3. The MnO_x/Al_2O_3 catalyst improves the NO_x production rate by ~ 60% compared to Al_2O_3, which is much higher than the reported enhancement (at most 10%) of active metal oxides (e.g., WO_3) supported on Al_2O_3 [15].

Figure 5 shows the effect of N_2 content on NO_x production in the packed-bed DBD reactor. The discharge powers are very close at the same input power, as shown in Fig. S5. With the increase of N_2 content from 40 to 90%, NO_x concentrations present volcano-shaped variation, and the peak concentrations of NO_x fall in the N_2 content range from 50 to 70%. Within the investigated range of N_2 content, MnO_x/Al_2O_3 catalyst exhibits much higher NO_x concentration than Al_2O_3.

According to NO_x concentration and total flow rate in Fig. 5a, the ratio of NO_x production rate of MnO_x/Al_2O_3 to Al_2O_3 versus N_2 content is shown in Fig. 5b. As N_2 content increases from 40 to 90%, NO_x production rate ratio of MnO_x/Al_2O_3 to Al_2O_3 climbs linearly from 1.3 to 1.6. It can be concluded that MnO_x/Al_2O_3 catalyst displays greater enhancement on NO_x production at higher N_2 content (lower O_2 content).

To gain an insight on the enhanced effect of MnO_x/Al_2O_3 catalyst, its electrical discharge characteristics, OES and surface role of the catalyst were further investigated.

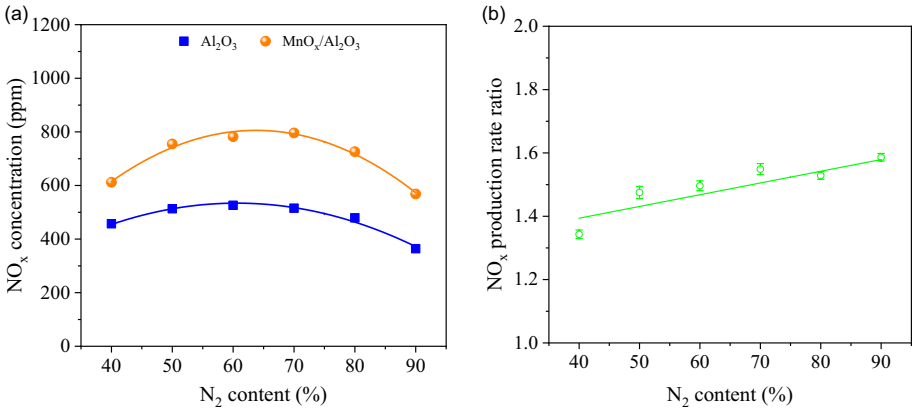

Fig. 5 Effect of N_2 content on **a** NO_x concentration and **b** NO_x production rate ratio of MnO_x/Al_2O_3 to Al_2O_3. Conditions: $P_{in} = 20$ W, $F_{in} = 600$ SCCM, P_{dis} is shown in Fig. S5

Electrical Discharge Characteristics and OES Diagnostic

Figure 6 shows the waveforms of current–voltage for the empty, Al_2O_3-packed, or MnO_x/Al_2O_3-packed DBD reactors. The corresponding charge–voltage Lissajous figures for the three cases are displayed in Fig. 7, obtaining their discharge powers of about 17 W. The current pulses variation with time in Fig. 6 and the discharge appearance in Fig. S6 indicate that the discharge is in the typical filamentary mode with a large amount of micro-discharges [24]. In the case of the MnO_x/Al_2O_3-packed DBD, the filamentary discharge becomes weak micro-discharge along with surface discharge. The current waveforms between empty DBD and Al_2O_3-packed DBD are very similar, there existing tens of current pulses in a quarter cycle of applied voltage, and the Lissajous figures are similar to parallelogram (Fig. 7). In contrast, the MnO_x/Al_2O_3-packed DBD exhibits more current pulses with lower intensity (Fig. S7) and the Lissajous figure becomes a distorted parallelogram. The Lissajous figures show the relationship between the transferred charge in the circuit and the voltage applied to the DBD plasma. From the slope of the upper and lower edges of the parallelogram, the total capacitance of the DBD can be estimated. The MnO_x/Al_2O_3-packed DBD has larger total capacitance than the empty and Al_2O_3-packed DBD, which is caused by that MnO_x is a kind of semiconductor material. The peak-to-peak voltages are almost equal in the three cases in Fig. 7, but the peak-to-peak charge in the case of MnO_x/Al_2O_3 is greater than the other two cases. A similar phenomenon was observed in the $BaTiO_3$-packed DBD [16]. Compared with the empty and Al_2O_3-packed DBD, the MnO_x/Al_2O_3-packed DBD shows special discharge characteristics and features much more and lower-intensity micro-discharges, leading to an increase in collision probability of electrons and reactant molecules. This is advantageous to the generation of more active species and promotes the subsequent reaction for NO_x formation.

At the same conditions as Fig. 5, the variations in rotational temperature (T_r) and vibrational (T_v) temperatures of N_2 molecule from fitting the OES results with N_2 content are shown in Fig. 8. In the packed-bed DBD, the vibrational temperatures of MnO_x/Al_2O_3 are higher than those of Al_2O_3, with an average increase of about 230 K. The MnO_x/Al_2O_3-packed DBD features much more and lower-intensity micro-discharges, larger total capacitance and greater peak-to-peak charge than the Al_2O_3-packed DBD, leading to a somewhat

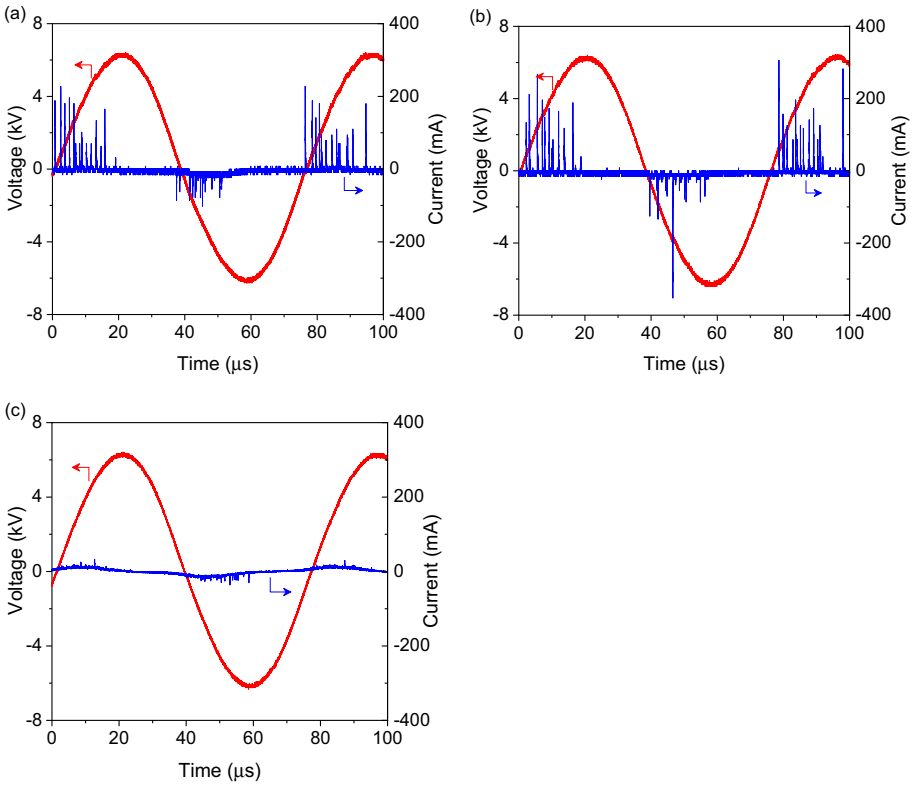

Fig. 6 Waveforms of applied voltage and discharge current in **a** empty, **b** Al_2O_3-packed and **c** MnO_x/Al_2O_3-packed DBD. Conditions: F_{in} = 600 SCCM, 50% N_2 + 50% O_2, P_{in} = 30 W

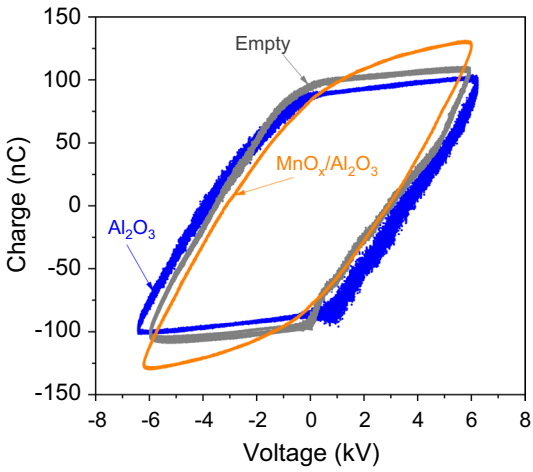

Fig. 7 Lissajous figures of empty, Al_2O_3-packed and MnO_x/Al_2O_3-packed DBD (corresponding discharge power of 16.8, 16.9 and 17.3 W, respectively). Conditions: F_{in} = 600 SCCM, 50% N_2 + 50% O_2, P_{in} = 30 W

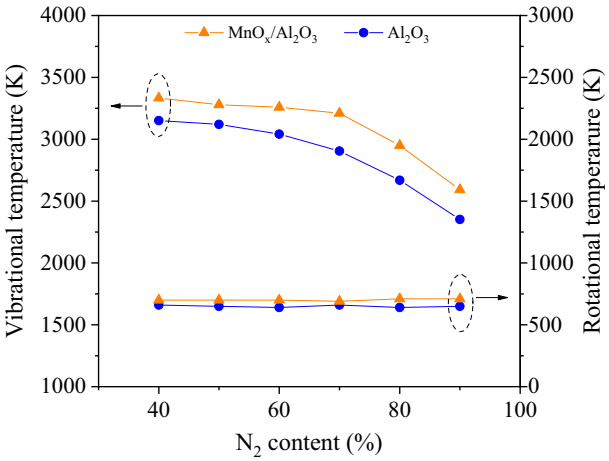

Fig. 8 Dependence of rotational and vibrational temperatures of the packed-bed DBD upon N_2 content. Conditions: $F_{in}=600$ SCCM, $P_{in}=20$ W, P_{dis} is given in Fig. S5

increase in electron density. This is favorable to forming more vibrationally-excited nitrogen molecules with high vibration quantum number, thus bring about a rise in the vibrational temperature of MnO_x/Al_2O_3. The differences in rotational temperature between MnO_x/Al_2O_3 and Al_2O_3 are not significant, and they are equivalent if considering fitting deviation.

For the packed-bed DBD, the rotational temperature is independent of N_2 content. By contrast, the vibrational temperature decreases with N_2 content probably due to the decrease of average energy per N_2 molecule from vibrational excitation. The lower T_v at higher N_2 content suggests that the populations of the high-lying vibrational levels of N_2 decline with the number of N_2 molecules.

Insight into Surface Role of MnO_x/Al_2O_3 Catalyst in the NO_x Production

To gain an insight into surface role of MnO_x/Al_2O_3 catalyst in the NO_x production, the two-step surface reaction processes and in-situ TPD for the adsorbed species of the first step were implemented. For MnO_x/Al_2O_3, after the first step of O_2 adsorption or O_2 plasma, the MS signal during the second step of N_2 plasma is shown in Fig. 9a, b, respectively. MnO_x/Al_2O_3 catalyst in N_2 plasma after O_2 adsorption is unable to produce NO (Fig. 9a). However, after O_2 plasma, NO can be produced significantly in N_2 plasma and plenty of O_2 is released from the oxygen species adsorbed on MnO_x/Al_2O_3 surface (Fig. 9b). This indicates that the oxygen species involved in production of NO and O_2 in Fig. 9b derive from O_2 plasma, rather than from O_2 adsorption. As expected, on the Al_2O_3 surface, there is no production of NO and O_2 even after O_2 plasma (Fig. 9c). It can be concluded that O_2 plasma results in the production of oxygen species on MnO_x surface, providing the required oxygen source for the formation of NO in N_2 plasma. The conclusion is confirmed again by in-situ TPD for the adsorbed species of the first step. The MnO_x/Al_2O_3 catalyst after O_2 plasma presents obviously a desorption peak of O_2 at 652 K, compared with that after O_2 adsorption (Fig. 10a). In contrast, there is no desorption peak of N_2 on the MnO_x/Al_2O_3 catalyst, whether after N_2 plasma or after N_2 adsorption (Fig. 10b).

When MnO_x/Al_2O_3 catalyst is exposed to O_2 plasma, the oxygen vacancies on MnO_x surface may serve as the active sites of the excited-state oxygen molecules (O_2^*) produced

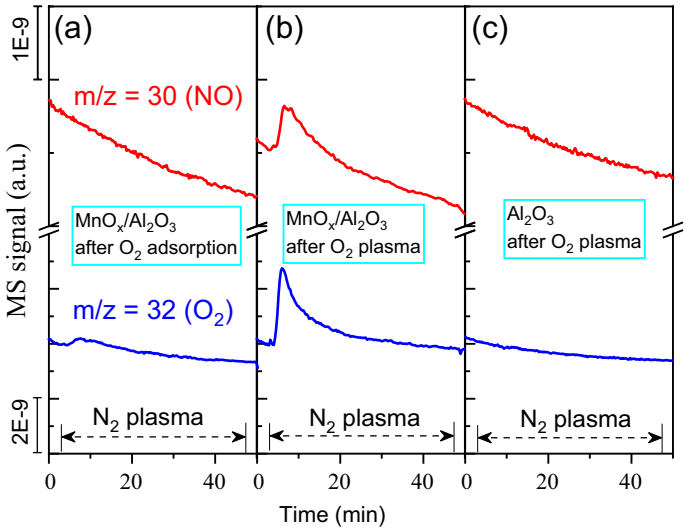

Fig. 9 MS signals of m/z = 30 (NO) and m/z = 32 (O_2) from N_2 plasma: **a** MnO_x/Al_2O_3 after O_2 adsorption, **b** MnO_x/Al_2O_3 after O_2 plasma, and **c** Al_2O_3 after O_2 plasma. Conditions: O_2 adsorption (F_{in} = 100 SCCM, 20 min); O_2 plasma (F_{in} = 100 SCCM, P_{in} = 20 W, 20 min); N_2 plasma (F_{in} = 100 SCCM, P_{in} = 20 W, 45 min)

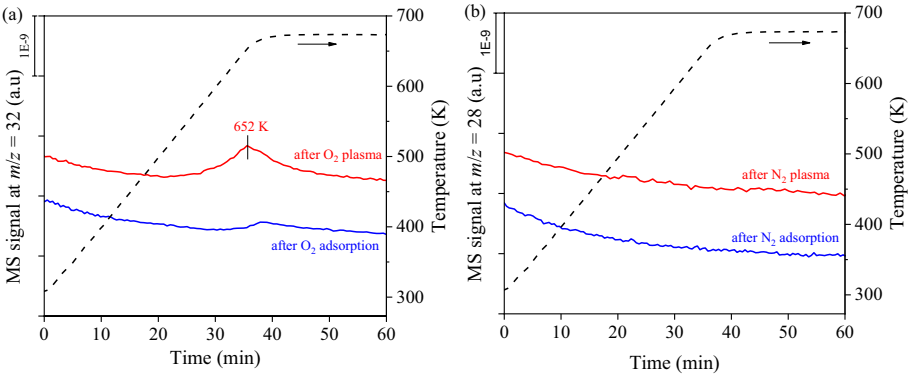

Fig. 10 MS signals of TPD at **a** m/z = 32 after O_2 plasma or adsorption, and **b** m/z = 28 after N_2 plasma or adsorption on MnO_x/Al_2O_3 catalyst. Conditions (before TPD): O_2 or N_2 plasma (F_{in} = 100 SCCM, P_{in} = 20 W, 20 min); O_2 or N_2 adsorption (F_{in} = 100 SCCM, 20 min)

from plasma, which may be electronically (e.g., metastable-state $O_2(^1\Delta_g)$) and vibrationally excited. The O_2^* species on MnO_x/Al_2O_3 catalyst becomes adsorbed oxygen atoms (O_{ad}) by dissociation adsorption.

If the MnO_x/Al_2O_3 catalyst is only exposed to N_2 gas after O_2 plasma, there is no NO production, as shown in Fig. S8a, confirming that the adsorbed oxygen atoms (O_{ad}) on MnO_x/Al_2O_3 catalyst has no efficient energy to react with ground-state N_2 molecule. This implies that the O_{ad} species on MnO_x/Al_2O_3 catalyst can only react with the excited-state nitrogen molecules (N_2^*) produced from plasma, including electronically (e.g.,

metastable-state $N_2(A^3\Sigma_u^+)$, $N_2(B^3\Pi_g)$, $N_2(C^3\Pi_u)$) and vibrationally (N_2 (v)) excited nitrogen molecules.

Furthermore, if the MnO_x/Al_2O_3 catalyst, after exposure to N_2 plasma of the first step, is incapable of producing NO in O_2 plasma of the second step, as shown in Fig. S8b. It is evidenced that the N_2^* species are unable to adsorb on MnO_x/Al_2O_3 catalyst (Fig. 10b), due to the very low dissociative sticking probability [25]. It can be concluded that the O_2^* species in plasma may turn into the atomic oxygen species (O_{ad}) adsorbed on MnO_x/Al_2O_3 catalyst by means of dissociation adsorption, and then the O_{ad} species react with the N_2^* species coming from plasma to form NO, as illustrated in Fig. 11. The contribution of MnO_x/Al_2O_3 catalyst to NO_x formation becomes greater under lower O_2 content (higher N_2 content), which is consistent with the dependence of enhancement of MnO_x/Al_2O_3 on N_2 content in Fig. 5b.

Conclusions

Based upon the comparison with the empty and Al_2O_3-packed DBD, an enhanced effect on NO_x production in MnO_x/Al_2O_3-packed DBD is reported. At N_2 content of 50% and *SEI* of ~ 16 kJ/mol (flow rate of 800 SCCM and discharge power of ~ 9.5 W), NO_x production rates are 0.28 SCCM for Al_2O_3-packed and 0.42 SCCM for MnO_x/Al_2O_3-packed.

When the flow rate is fixed, the NO_x concentration and production rate increase rapidly with *SEI*. In contrast, when the flow rate is changed, the NO_x production rate rises very slow with *SEI* for Al_2O_3-packed, and even turns to decrease slightly after a small increase for MnO_x/Al_2O_3-packed. NO_x concentration presents volcano-shaped variation with N_2 content and the peak concentrations of NO_x fall in N_2 contents of 50–70%. As N_2 content increases from 40 to 90%, NO_x production rate ratio of MnO_x/Al_2O_3 to Al_2O_3 grows

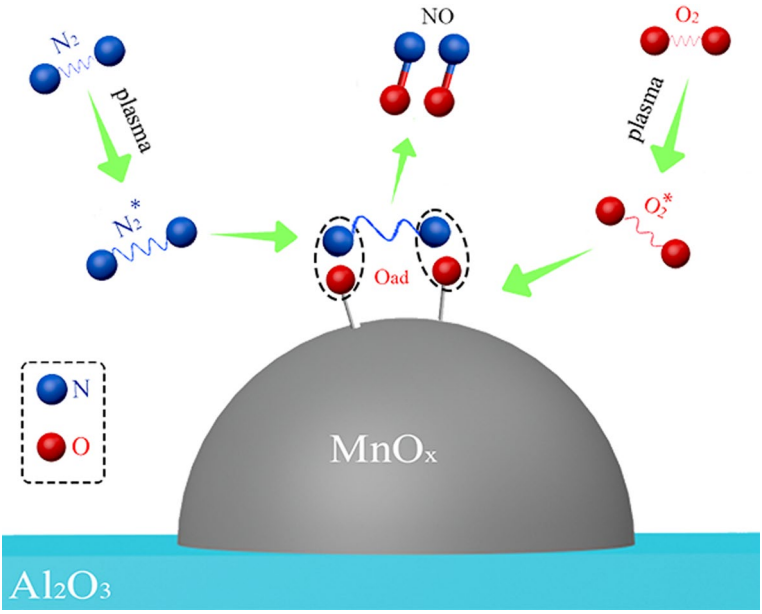

Fig. 11 Illustrating the surface contribution to MnO_x/Al_2O_3-enhanced NO_x production

linearly from 1.3 to 1.6. In brief, the enhanced effect becomes more significant at lower *SEI* or higher N_2 content (lower O_2 content).

The MnO_x/Al_2O_3-packed DBD features much more and lower-intensity micro-discharges, larger total capacitance and greater peak-to-peak charge than the Al_2O_3-packed DBD, forming more vibrationally-excited nitrogen molecules with high vibration quantum number, thus bring about a rise in the vibrational temperature of MnO_x/Al_2O_3. The surface role of MnO_x/Al_2O_3 catalyst in the enhanced effect was disclosed by two-step surface reaction processes and in-situ TPD for the adsorbed species of the first step. The O_2^* species in plasma may turn into the O_{ad} species on MnO_x/Al_2O_3 catalyst by means of dissociation adsorption, and then the O_{ad} species react with the N_2^* species coming from plasma to form NO.

Supplementary Information The online version contains supplementary material available at https://doi.org/10.1007/s11090-023-10345-8.

Author Contributions TQZ: Investigation, Data curation, Validation, Writing—Original draft. XSL, JLL and XQW: Methodology, Formal analysis, Visualization, Writing—Reviewing and Editing. AMZ: Conceptualization, Supervision, Resources, Funding acquisition, Writing- Reviewing and Editing.

Funding This work is supported by the National Natural Science Foundation of China (22278052, 11975069) and the Liaoning Revitalization Talent Program (XLYC2008032).

Data Availability Data are available on request from the authors.

Declarations

Conflict of interests The authors have no competing interests to declare that are relevant to the content of this article.

Ethical Approval Not applicable.

References

1. Patil BS, Wang Q, Hessel V, Lang J (2015) Plasma N_2-fixation: 1900–2014. Catal Today 256:49–66
2. Abdelaziz AA, Ishijima T, Osawa N, Seto T (2019) Quantitative Analysis of ozone and nitrogen oxides produced by a low power miniaturized surface dielectric barrier discharge: effect of oxygen content and humidity level. Plasma Chem Plasma Process 39:165–185
3. Abdelaziz AA, Kim HH (2020) Temperature-dependent behavior of nitrogen fixation in nanopulsed dielectric barrier discharge operated at different humidity levels and oxygen contents. J Phys D Appl Phys 53:17
4. Han YF, Wen SY, Tang HW, Wang XH, Zhong CS (2018) Influences of frequency on nitrogen fixation of dielectric barrier discharge in air. Plasma Sci Technol 20:7
5. Zhang S, Zong LJ, Zeng X, Zhou RW, Liu Y, Zhang C, Pan J, Cullen PJ, Ostrikov K, Shao T (2022) Sustainable nitrogen fixation with nanosecond pulsed spark discharges: insights into free-radical-chain reactions. Green Chem 24:1534–1544
6. Van Alphen S, Eshtehardi HA, O'Modhrain C, Bogaerts J, Van Poyer H, Creel J, Delplancke MP, Snyders R, Bogaerts A (2022) Effusion nozzle for energy-efficient NOx production in a rotating gliding arc plasma reactor. Chem Eng J 443:12
7. Jardali F, Van Alphen S, Creel J, Eshtehardi HA, Axelsson M, Ingels R, Snyders R, Bogaerts A (2021) NOx production in a rotating gliding arc plasma: potential avenue for sustainable nitrogen fixation. Green Chem 23:1748–1757
8. Vervloessem E, Aghaei M, Jardali F, Hafezkhiabani N, Bogaerts A (2020) Plasma-based N_2 fixation into NOx: insights from modeling toward optimum yields and energy costs in a gliding arc plasmatron. ACS Sustain Chem Eng 8:9711–9720

9. Gorbanev Y, Vervloessem E, Nikiforov A, Bogaerts A (2020) Nitrogen fixation with water vapor by nonequilibrium plasma: toward sustainable ammonia production. ACS Sustain Chem Eng 8:2996–3004
10. Wang WZ, Patil B, Heijkers S, Hessel V, Bogaerts A (2017) Nitrogen fixation by gliding arc plasma: better insight by chemical kinetics modelling. Chemsuschem 10:2145–2157
11. Lu X, Bruggeman PJ, Reuter S, Naidis G, Bogaerts A, Laroussi M, Keidar M, Robert E, Pouvesle J-M, Liu D, Ostrikov K (2022) Grand challenges in low temperature plasmas. Front Phys 10:1040658
12. Liu TW, Gorky F, Carreon ML, Gomez-Gualdron DA (2022) Energetics of reaction pathways enabled by N and H radicals during catalytic, plasma-assisted NH_3 synthesis. ACS Sustain Chem Eng 10:2034–2051
13. Rapakoulias D, Cavadias S, Amouroux J (1980) Processus catalytiques dans un réacteur à plasma hors d'équilibre II. Fixation de l'azote dans le système N_2–O_2. Rev Phys Appl 15:1261–1265
14. Gicquel A, Cavadias S, Amouroux J (1986) Heterogeneous catalysis in low-pressure plasmas. J Phys D Appl Phys 19:2013
15. Patil BS, Cherkasov N, Lang J, Ibhadon AO, Hessel V, Wang Q (2016) Low temperature plasma-catalytic NO_x synthesis in a packed DBD reactor: effect of support materials and supported active metal oxides. Appl Catal B 194:123–133
16. Ma Y, Wang Y, Harding J, Tu X (2021) Plasma-enhanced N2 fixation in a dielectric barrier discharge reactor: effect of packing materials. Plasma Sources Sci Technol 30:105002
17. Sun Q, Zhu AM, Yang XF, Niu JH, Xu Y (2003) Formation of NO_x from N_2 and O_2 in catalyst-pellet filled dielectric barrier discharges at atmospheric pressure. Chem Commun 9:1418–1419
18. Dong Y, Sun J, Ma X, Wang W, Song Z, Zhao X, Mao Y, Li W (2022) Study on the synergy effect of MnO_x and support on catalytic ozonation of toluene. Chemosphere 303:134991
19. Zhao TL, Xu Y, Song YH, Li XS, Liu JL, Liu JB, Zhu AM (2013) Determination of vibrational and rotational temperatures in a gliding arc discharge by using overlapped molecular emission spectra. J Phys D Appl Phys 46:345201
20. Gershman S, Fetsch H, Gorky F, Carreon ML (2022) Identifying regimes during plasma catalytic ammonia synthesis. Plasma Chem Plasma Process 42:731–757
21. Cheng H, Li Y, Zheng K, Liu D, Lu X (2021) Numerical analysis of nitrogen fixation by nanosecond pulse plasma. J Phys D Appl Phys 54:184003
22. Katabathini N, Maksod IHAE, Mokhtar M (2021) Cu, Fe and Mn oxides intercalated SiO_2 pillared magadiite and ilerite catalysts for NO decomposition. Appl Catal A 616:118100
23. Goto N, Kudo S, Motoyama H, Ohyama S (2002) Direct decomposition technique for NO in O_2–N_2 mixture using barrier discharge and Cu zeolite. Jpn J Appl Phys Part 2 41:L64–L66
24. van't Veer K, van Alphen S, Remy A, Gorbanev Y, De Geyter N, Snyders R, Reniers F, Bogaerts A (2021) Spatially and temporally non-uniform plasmas: microdischarges from the perspective of molecules in a packed bed plasma reactor. J Phys D Appl Phys 54:174002
25. Rouwenhorst KHR, Jardali F, Bogaerts A, Lefferts L (2021) From the Birkeland-Eyde process towards energy-efficient plasma-based NOx synthesis: a techno-economic analysis. Energy Environ Sci 14:2520–2534